Inception of stream incision by seepage erosion

A. Pornprommin[1] and N. Izumi[2]

Received 28 April 2009; revised 26 October 2009; accepted 11 January 2010; published 26 June 2010.

[1] Because seepage erosion is generated by complex interactions with other processes, associated stream incision process is not well understood. In this study, some fundamental characteristics of incipient incision by seepage erosion were investigated by laboratory experiments and linear stability analysis. The experiments were conducted with various sediment layer depths and gradients. With similar discharges in the experiments, incision spacing decreases with increasing depth of the sediment layer and with increasing gradient, whereas incision width increases with increasing sediment layer depth. A linear stability analysis was performed using the Dupuit-Forchheimer equation and an expression of the planimetric retreat of the scarp. The retreat velocity of the scarp consists of two terms: (1) a power law function that describes the specific discharge in excess of a critical discharge and (2) a diffusion-like function that describes the incision edge shapes, in which the retreat rate is enhanced or reduced by the convexity and concavity of the edges, respectively. This analysis shows that the characteristic incision spacing becomes infinitely small when the effect of the edge shapes is excluded. Using the experimental data of incision spacings, the values of the diffusion-like coefficient in the second term were estimated. Since the weight of a failure block and hydraulic pressure are the driving forces in the slope stability analysis, a relationship was found between the diffusion-like coefficient and the combination of the two forces.

Citation: Pornprommin, A., and N. Izumi (2010), Inception of stream incision by seepage erosion, *J. Geophys. Res.*, *115*, F02022, doi:10.1029/2009JF001369.

1. Introduction

[2] Flow concentration may cause small rills or incisions that represent the initial or early stages of gully development. By widening, deepening, and headcut formation, gullies cause severe soil erosion that adversely affects agricultural productivity, limits land use, and threatens roads and structures. Soil eroding from gullied areas induce high rates of sediment runoff and cause rapid siltation and bed aggradation downstream. Furthermore, there is the possibility that nutrients and pesticides attached to the eroded and suspended sediment will result into water quality degradation [*Carey*, 2006]. Thus, a better understanding of the incision processes is vital, not only for geologists but also for researchers in various other fields, such as civil engineering and land use planning.

[3] A gully is defined as a steep-sided incision with an eroding headcut and slumping sidewalls [*Bradford and Piest*, 1980; *Schumm et al.*, 1984]. *Bull and Kirkby* [1997] listed the following processes affecting gully morphology: overland flow, hillslope infilling, pipe initiation, pipe enlargement by flow, mass failures, and the magnitude of storm events. They mentioned that there are gaps in the understanding of mass failures and gully formation by seepage. According to *Dunne* [1990], *Lamb et al.* [2006], and *Luo and Howard* [2008], groundwater that emerges from rock or sediment is termed seepage. The removal of mass from a seepage face by exfiltrating water is termed seepage erosion, whereas weathering processes that are facilitated by seepage (e.g., salt precipitation, chemical dissolution or frost growth) are termed seepage weathering. Fluvial erosion, erosion of a bank or gully toe by streamflow or concentrated flow of runoff, can also cause undercutting of a bank or gully wall. Seepage erosion describes a process that undercuts a bank by seepage, as opposed to fluvial erosion. Therefore, mass failure of the bank or gully wall can be induced by either process. For several decades, many researchers attempted to describe the role of seepage erosion, the morphologic features by seepage, and the dissimilarity from the features generated by surface flow [e.g., *Dunne*, 1980; *Higgins*, 1982, 1984; *Laity and Malin*, 1985; *Pillans*, 1985; *Schumm and Phillips*, 1986; *Kochel and Piper*, 1986; *Luo*, 2000; *Hoke et al.*, 2004]. However, *Lamb et al.* [2006] argued that some fluvial features, such as waterfalls and plunge pools, are also capable of carving out amphitheater-like valley heads, often related to seepage erosion, and found little evidence existing for seepage erosion in basaltic valleys on Earth. Recently, *Luo and Howard* [2008] proposed that the valley networks observed

[1]Department of Water Resources Engineering, Kasetsart University, Bangkok, Thailand.
[2]Department of Civil Engineering, Hokkaido University, Sapporo, Japan.

0148-0227/10/2009JF001369

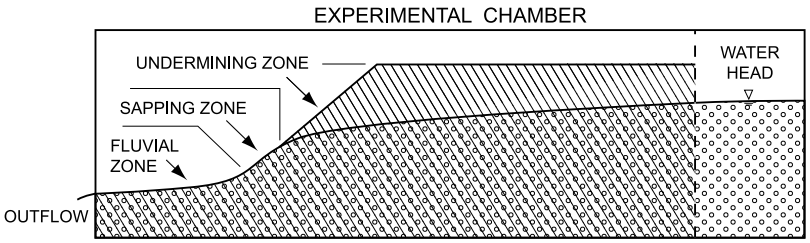

Figure 1. Experimental seepage erosion chamber, showing major process zones (undermining, sapping, and fluvial zones) at the downstream face of the sediment layer. Stippled areas are sediment; circles show the saturated zone. The permeable screen (dashed line) permits water to flow from the water head reservoir into the sediment (modified from *Howard and McLane* [1988]).

on the planet Mars may be generated by fluvial erosion and seepage weathering. Seepage weathering weakens the rock in canyon headwalls, and therefore enhances fluvial erosion in bedrock. Although the roles of seepage erosion in bedrock are not clearly known, seepage erosion is accepted as an important contributing factor of rill, gully, and stream bank erosion in sediment [e.g., *Abam*, 1993; *Chu-Agor et al.*, 2008b; *Dietrich and Dunne*, 1993; *Schumm et al.*, 1995; *Sultan et al.*, 2004; *Wilson et al.*, 2007].

[4] In comparison with overland flow, relatively few studies have focused on incision due to seepage erosion. *Howard and McLane* [1988] conducted a series of seepage erosion experiments in a narrow chamber (two-dimensional experiment), and distinguished three major process zones on a seepage surface (Figure 1). The sapping zone is the narrow surface area at the upstream end of the emerging seepage flow where most of the seepage erosion is concentrated due to strong seepage forces. The undermining zone lies on top of the sapping zone, and particle detachment and removal in the sapping zone results in intermittent mass failure of this zone. In the fluvial zone, downstream from the sapping zone, the seepage force is small, and sediment is transported by fluvial processes. They also suggested that the total sediment movement at a seepage face consists of the sum of the fluvial and mass-wasting transports. *Howard* [1988] conducted his experiments in a 5 foot (approx. 1.5 m) wide chamber (three-dimensional experiment) with both cohesionless and slightly cohesive sand. He found that a higher flow rate produced an incision of greater width and increased the activity of the incision head, and that the incisions became narrower and deeper when slightly cohesive sand was used. *Kochel and Piper* [1986] conducted their experiments using fine and coarse sand in a 2.5 m wide flume. They related incision development to the effects of structural and/or stratigraphic variations in sediment layers in order to mimic their observations on incision development in Hawaii. *Gomez and Mullen* [1992] conducted experiments in a sand filled V-shaped cross section (1.8 m wide drainage area) to encourage the development of a central trunk stream. They proposed that drainage network evolution due to seepage erosion can be described by three phases. In the first phase of evolution (initiation), the drainage network grew headward rapidly. Then, the network expanded through tributary growth and lateral valley wall retreat (extension phase). Finally, in the phase of abstraction, the divides between lateral valleys decayed due to valley widening. They also observed that basin sediment discharge declined exponentially with time. *Huang and Laflen* [1996] investigated the effects of seepage on erosion of a clay loam soil in a 5 m long, 1.2 m wide soil box under both rainfall and surface flow. They observed that soil moisture had a significant influence on the erosion rate, and seepage greatly increased soil erosion due to headcut development. *Owoputi and Stolte* [2001] examined the role of seepage using a laboratory flume subjected to variable seepage and rainfall conditions and three slope gradients. They found that seepage alone had little effect on erosion rate, but it significantly affects the erodibility of both sand and sandy clay till. *Schorghofer et al.* [2004] reproduced the development of incisions or rills in a 120 cm wide, tabletop apparatus, and suggested that incisions by surface flow grew due to seepage erosion. Incision frequency was related to length, and there was a characteristic frequency spacing. Using the same experimental apparatus, *Lobkovsky et al.* [2004, 2007] also studied the onset of seepage erosion and incision growth. *Fox et al.* [2006, 2007] studied seepage particle mobilization and undercutting using a two-dimensional soil lysimeter and derived a seepage erosion sediment transport function with an excess discharge formulation. Recently, *Chu-Agor et al.* [2008a] conducted experiments in a 50 cm wide chamber, studied headcut formation in detail, and suggested that seepage causes hillslope instability through three different factors: soil pore water pressure, seepage gradient forces, and seepage particle detachment and removal. As seepage erosion is generated by the complex interaction among seepage and other mechanisms, more detailed work is needed to fully understand the roles of seepage on slope instability and incision development.

[5] From a theoretical viewpoint, incision and rill development as a result of seepage erosion has received much less attention than incision and rills due to overland flow. One of the earliest studies of incision development by overland flow was conducted by *Smith and Bretherton* [1972] using a stability analysis. In the analysis, small sinusoidal perturbations with various wave numbers were imposed in the lateral direction on a tilted plateau, and the growth of these perturbations was investigated. If the growth rate of a perturbation was positive, it means that perturbation could grow into large amplitude incisions. Since wave length corresponds to incision spacing, the wavelength associated with the maximum positive growth rate was assumed to be the incision spacing that appeared in the field (characteristic spacing). Although the predicted spacing was found to be infinitely small due to the assumption of steady uniform open channel flow, their groundbreaking work motivated many other studies [*Luke*, 1974; *Loewenherz*, 1991; *Loewenherz-*

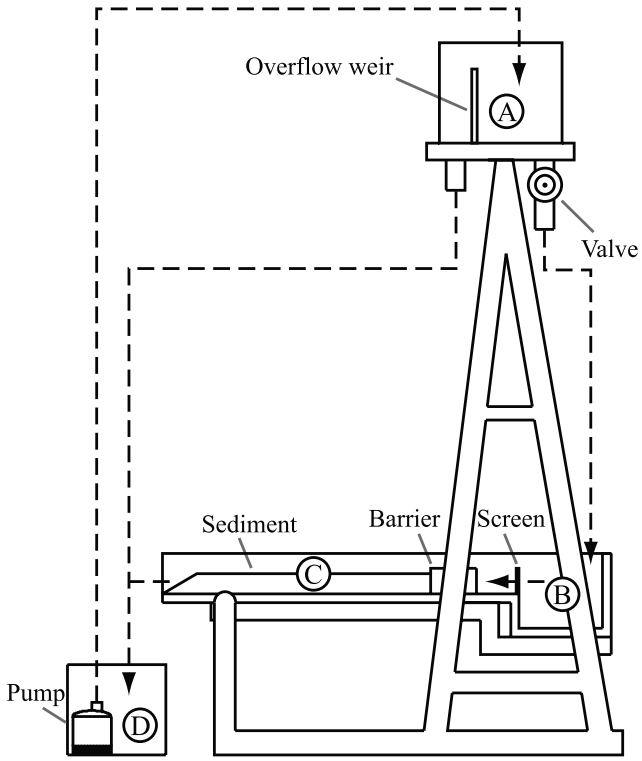

Figure 2. Side view of a seepage erosion apparatus; dashed lines with arrows show directions of water flow. Labels are as follows: A is the top tank, B is the upstream reservoir, C is the experimental chamber, and D is the downstream reservoir.

Lawrence, 1994; *Izumi and Parker*, 1995; *Revelli and Ridolfi*, 2001; *Fowler et al.*, 2007]. Currently, the theory is being advanced that rill incisions caused by overland flow can be approached with standard linear stability analysis, in which the finite, characteristic incipient incision spacing can be determined [*Izumi and Parker*, 2000; *Izumi and Fujii*, 2006; *Pornprommin et al.*, 2009]. In addition, *Izumi* [2004] performed a linear stability analysis to investigate the formation of submarine gullies caused by turbidity currents. To the authors' knowledge, however, linear stability analysis has never been applied in incision processes causing by seepage erosion.

[6] In this study, we present a three-dimensional experiment in order to investigate certain factors, namely, sediment layer depth and gradient that may control the inception and evolution of incision development by seepage erosion. Following an idea formulated by *Howard* [1988, 1995], the first linear stability analysis of channelization by seepage erosion was performed based on the planimetric shape of the incision edge in order to investigate incipient incision spacing. Finally, using the experimental data of incision spacings, we apply dimensional analysis theory to derive a tentative relationship between the diffusion-like coefficient controlling incipient incisions and the combination of driving forces.

2. Seepage Experiment

2.1. Experimental Setup and Data Collection

[7] The side view of the seepage erosion apparatus used in this experiment is shown in Figure 2. The directions of water flow are indicated, and A, B, C and D represent the top tank, the upstream reservoir, the experimental chamber and the downstream reservoir, respectively. In the top tank (A), a constant water level is maintained by an overflow weir. Water discharge from the top tank flowing down to the upstream reservoir (B) is controlled by a valve. When the water level in the upstream reservoir reaches a sufficient height, water overflows through a narrow-opening screen into the experimental chamber (C). The screen is used to create a laterally uniform flow. Before the water reaches the upstream face of the sediment layer, it flows through a wire mesh barrier, used to support the sediment layer. The sediment layer is 150 cm wide and 120 cm long, but the depth varies, so that the effects of various sediment layer depths could be investigated. In addition, the chamber can be tilted to the desired slope. Considering a chamber bed as an impermeable, nonerodible layer, we can study the effects of the two-layer alignment (sediment layer and impermeable layer) by varying the chamber slope. Sand grains were glued to the surface of the chamber bed to increase the friction between the sediment layer and the chamber bed. On the downstream face of the sediment layer a scarp was created with a slope of 1:1.5 (vertical:horizontal) in reference to the chamber bed. In every experiment, groundwater flowed through the sediment layer under the upland surface and emerged at the scarp where, at certain unspecified locations, incisions developed due to seepage erosion. In this study, there was no overland flow on the top of the sediment layer. Seepage flow and the entrained sediment dropped down to the downstream reservoir (D), where water was recirculated to the top tank (A) by a pump.

[8] Cohesionless artificial plastic pellets (Acrylic, PMMA) were used as sediment in this study. Each pellet has the shape of an elliptical cylinder with a major axis of 3 mm, a minor axis of 2 mm, and a height of 3 mm. The specific gravity was 1.19, and the angle of the dry pellets at rest was approximately 54°. Although the plastic pellets have many different properties from real soils such as particle density, surface tension, and permeability, there are some advantages using plastic pellets. The effects of soil cohesion, compaction, and creep can be minimized. Moreover, because of low particle density, the erosion rates are very high, and that facilitates many experiments. However, experiments using real soils should be conducted in the future for better understanding of the real complex interactions between seepage erosion and other processes in nature. In order to enable the pellets to be reused without delay, we mixed them with water so that a similar moisture condition would be created each time a new experiment was started. The pellets completely covered the bed, and they were randomly distributed. During the experiment, discharge of water was controlled with a valve connecting the top tank and the upstream reservoir. If active erosion did not take place, water discharge was programmed to gradually increase every five minutes. The advantage of our system is that it enables a constant discharge during operation. Two CCD cameras, installed above and in front of the sediment layer, were used to capture the development of incisions every 15 and 30 s, respectively. A digital video camera was also used to examine seepage erosion characteristics in greater detail. Where there was no active erosion, the discharge was

Table 1. Experimental Cases With Various Sediment Layer Depths and Chamber Slopes

Chamber Slope	Number of Experiments
6 cm[a]	
0.053	1
0.107	1
0.161	1
0.214	1
0.266	1
0.317	1
0.367	1
8 cm[a]	
0.053	1
0.107	2
0.161	2
0.214	1
0.266	1
0.317	1
0.367	1
10 cm[a]	
0.053	1
0.107	1
0.161	2
0.214	2
0.266	2
0.317	2
0.367	1

[a]Layer depth.

measured every five minutes by collecting the water that flowed down to the downstream reservoir.

[9] As shown in Table 1, the experiments consisted of three sediment layer depths of 6, 8 and 10 cm, respectively, and seven chamber slope gradients between 0.053 and 0.367 (totally 21 cases). In some cases, however, the experiments were repeated, so that a total of 27 experiments were conducted.

2.2. Experimental Results

2.2.1. Common Characteristics of Incision Evolution

[10] Since the threshold discharge for seepage erosion was investigated in this study, a small water discharge was allowed to flow through the sediment layer at the beginning of each experiment. Then, water discharge increased during the experiments until the incisions initiated. This water emerged at random places at the scarp and was collected at the downstream reservoir as water droplets. Some sediment at the toe of the scarp was removed by seepage erosion and flowed to the downstream reservoir. As discharge increased, the seepage increased and covered the entire area of the scarp toe forming a saturated sapping zone. The water droplets became streams of water, and more sediment in the sapping zone became entrained and flowed to the downstream reservoir. With further increases in discharge, seepage erosion increasingly undermined the scarp and finally induced small mass failures at various locations. When these mass failures initiated incisions and lowered the proximate water table, seepage at the incisions increased due to the concentration of groundwater flow. Thus, more seepage erosion and mass failures occurred and the incisions developed further by headcutting and widening. Seepage water along the incision edge especially at the incision heads transported the sediment from the fluvial zone to the downstream reservoir. At the same time, more sediment from the sapping zone was entrained to refill the loss in the fluvial zone. As a result, seepage erosion caused a change in the scarp geometry and generated further mass failures. The combined processes of seepage erosion and mass failure are similar to the processes described in the riverbank stability analysis by *Osman and Thorne* [1988]. However, we hypothesized that in the region of the incision sidewalls, mass failures are generated not only due to seepage erosion, but also from fluvial erosion resulting from flow in the incised area. We observed an increase in mass failures along the sidewalls when the flow in the incised areas shifted closer to the sidewalls. At times, intermittent tension cracks were clearly observed on the upslope surface approximately 1–3 cm from the incision edge prior to the occurrence of mass failures, and these were often found at the incision heads or at pointed scarps (headlands) where the edges extended out into the incised area. As a result, the overall planimetric shape of the incision edge is always concave.

[11] All incisions had amphitheater-shaped heads with steep sidewalls due to seepage erosion and mass failures (Figure 3). Experiments conducted in gently sloping conditions resulted in a greater water depth and volume of entrained sediment (Figure 3a). In contrast, on steeper gradients, the water depth was shallow and the chamber bed was exposed (Figure 3b). Moreover, three smaller incised areas

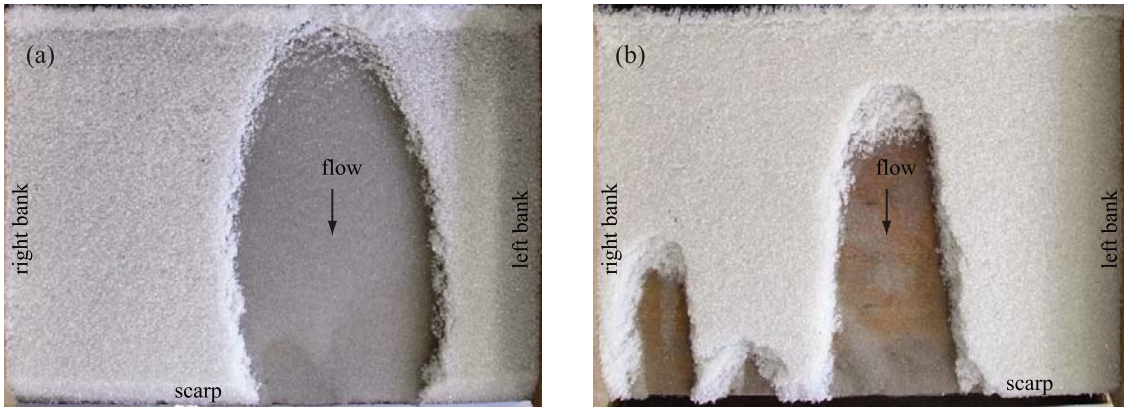

Figure 3. Plan views of stream incisions where sediment layer depth is 8 cm. (a) Slope is 0.053 at 29 min, 15 s, and (b) slope is 0.367 at 49 min.

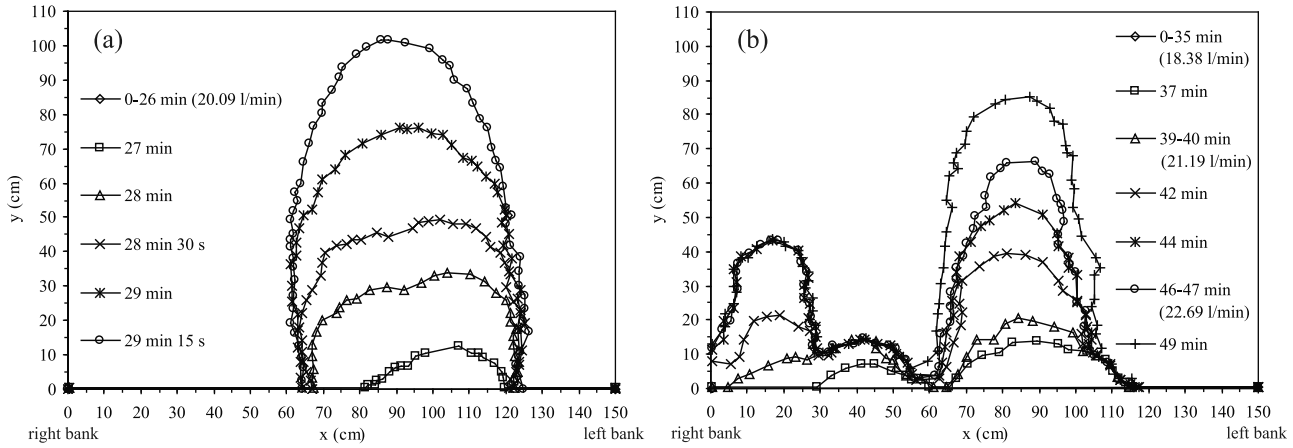

Figure 4. Temporal evolution of stream incisions corresponding to Figure 3 where the depth of the sediment layer is 8 cm. (a) Slope is 0.053, and (b) slope is 0.367.

can be seen in the steep gradient experiment (Figure 3b), whereas only one incision was visible in the gently sloping experiment (Figure 3a). *Chu-Agor et al.* [2008a] observed that seepage erosion on the scarp face initiated as unimodal (i.e., concentrated at one point) or multimodal (i.e., concentrated at several locations across the scarp face) features, controlled by the scarp angle. However, initial multimodal seepage erosion subsequently converted to unimodal seepage erosion sometime before mass failure. Thus, their results present insights into the mechanism of seepage erosion in the length scale of the mass failure. However, in our study, a larger length scale (i.e., scale of incision spacing) was considered.

[12] The gradient of the experiment shown in Figure 4a is gentle, and as a result, there is a considerable difference between the depth of the water in the groundwater in the sediment layer and that in the surface water downstream of the scarp. Thus, the influence of an incision on the groundwater flow field (flow concentration) increases as does the region in which groundwater can flow into the incision. We found that seepage erosion is very active and uniform after early incision development due to an increase in seepage flow at the incision head, which resulted in an incision with a symmetrical shape. Before an incision developed, a water discharge of 20.09 L/min was measured. Where the gradient of the chamber slope is very steep (Figure 4b), the flow concentration was weaker than that in the case of the gentle slope due to a smaller difference between the groundwater depth and the water depth downstream of the scarp. Moreover, the shallow surface flow caused the emergence of sediment in the fluvial zone downstream of the scarp. *Lamb et al.* [2008] indicated that the critical Shields parameter for incipient sediment motion for fluvial transport increases significantly if sediment emerges from water surface. We hypothesized that, due to an increase in this threshold value of the fluvial transport and a decrease in groundwater flow concentration, the seepage erosion observed in the steeper gradient experiment was rather limited (Figure 4b). Erosion did not occur uniformly and continuously along the scarp, rather appeared intermittently. Therefore, the incisions observed in the steep gradient experiment were less symmetrical (Figure 4b). Moreover, erosion ceased twice during the course of the experiment, and required an increase in water discharge in order to resume the evolution of the incisions. Although the both depth of the sediment layer and water discharge were similar in both experiments, a greater number of incisions was observed in the steeper slope case (Figure 4b). According to *Schorghofer et al.* [2004], flow concentration is an important factor in controlling incision spacing. For the steeper chamber slope, the difference in water depths between the upstream end and the scarp becomes smaller, and flow concentration becomes weaker. Thus, a greater number of incisions can be initiated compared to gentler gradients.

[13] If the entire land surface is covered with sufficient sediment deposits so that actual sediment transport rates equal to the transport capacities of flow, then the process is considered as a transport or energy-limited process. However, in many landscapes, the actual transport rates are considerably less than would be predicted for transport-limited processes. When bedrock is exposed on slopes, the rate of local erosion is determined by weathering rates. The volume of bed sediment transport by wash processes on hillslopes and low-order rills and channels is limited by the ability of the flow to entrain or erode regolith (residual soils or colluvium) or bedrock, giving detachment-limited (supply limited) conditions [e.g., *Howard*, 1994]. *Howard and McLane* [1988] observed that the capacity of fluvial transport of seepage flow to remove sediment eroded in the sapping zone controls seepage erosion (transport-limited process). However, in their experiments, the chamber bed was flat, and the sand on the bed was not completely removed by seepage erosion. Thus, the bed of the eroded area was always covered with sand and formed a specific longitudinal slope. For the gentle chamber slope experiments, the bed of the eroded area was covered with a very thin layer of sediment and the erosion was almost continuous. Thus, the process may be classified as transport limited similar to *Howard and McLane* [1988]. However, in the case of the steep chamber slope, the wood base of the chamber bed was exposed, and the erosion was intermittent. Thus, this process may be classified as detachment limited.

2.2.2. Incision Initiation

[14] Although the exact threshold water discharges could not be measured, they were estimated from average values

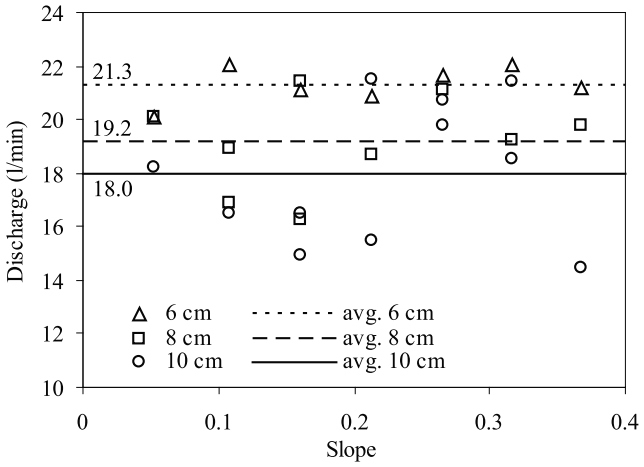

Figure 5. Threshold water discharge in the development of incisions in the experiments with chamber slopes from 0.053 to 0.367 and sediment layer depths of 6, 8, and 10 cm.

between the measured discharges before and after the initiation of incisions. The threshold water discharge was between 14.49 and 22.06 L/min (Figure 5), but no clear relationship was obtained between the chamber slope and the threshold water discharge. However, the average values of the threshold water discharge for sediment layer depths of 6, 8 and 10 cm were 21.29, 19.15 and 18.00 L/min, respectively. These results suggests that threshold water discharge increases with a decrease in the depth of the sediment layer. The possible reason for this is that an increase in depth may facilitate slope instability because the component of sediment weight along the failure plane is one of the driving forces in slope stability analysis.

2.2.3. Incision Width and Spacing

[15] The width of the dominant incision was related to the chamber slope and the sediment layer depth (Figure 6). The results of three experiments were omitted since the incisions which initiated at the edge of the chamber were likely not fully developed. The largest incision was chosen as the dominant one in each experiment. The results of the experiments indicated that the width of the incisions changed slightly once the incision developed, but that the length increased significantly with headcutting. Although no clear relationship between slope gradient and incision width was observed (Figure 6), the shapes as depicted in Figure 4 were less symmetrical on steeper slopes. In addition, average incision widths for sediment layer depths of 6, 8 and 10 cm, were 38.4, 54.6 and 58.0 cm, respectively, indicating that incision width increased with increasing sediment depth. It is possible that an increase in the sediment layer depth corresponded to the larger scale of mass failure, and the scale of mass failure may be related to the scale of the incision width.

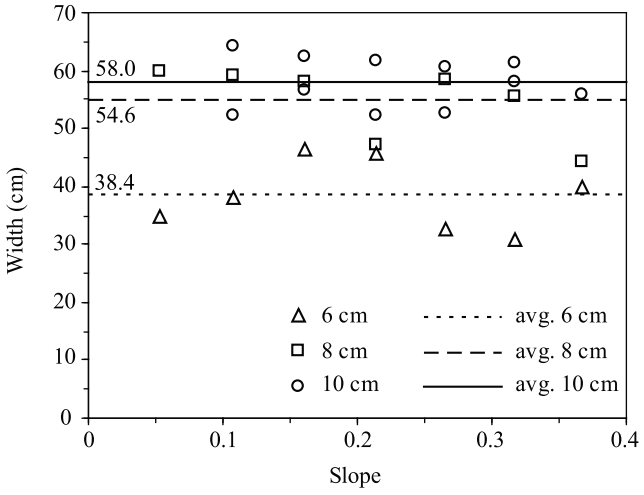

Figure 6. Dominant incision width in the experiments with chamber slopes from 0.053 to 0.367 and sediment layer depths of 6, 8, and 10 cm.

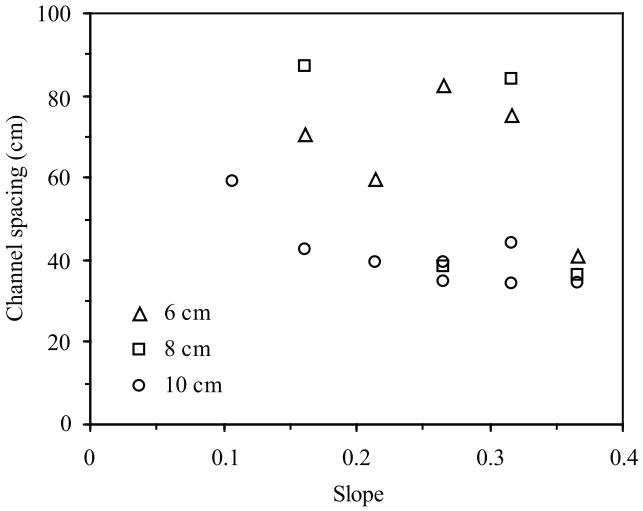

Figure 7. Incision spacing in the experiments with chamber slopes from 0.053 to 0.367 and sediment layer depths of 6, 8, and 10 cm.

[16] Incision spacing is defined as the distance between the centers of two neighboring incisions. If there is only one incision (i.e. experiment shown in Figures 3a and 4a), then no spacing can be determined, and if more than two incisions occur (Figures 3b and 4b), the average spacing value between neighboring incisions was used. Due to width restrictions in our apparatus, the maximum number of incisions in the experiments was no more than three. The observed incision spacing shows some fluctuations (Figure 7). If one incision initiates earlier than any other incisions, that initial incision becomes dominant and thus the incision spacing is relatively large when a small number of incisions initiate in the experimental chamber. Meanwhile, if more than one incision initiate virtually simultaneously, the spacing becomes relatively small. The number of incisions and the spacing at the final state are strongly influenced by the initial growth of incisions. Slight inaccuracies in the experimental configuration, such as sediment layer thickness, tend to effectively prevent simultaneous initiation of multiple incisions. We assume that, because it is difficult to eliminate inaccuracy in the experimental configuration, much scatter is observed in the incision spacing. In the experiments with the gentlest slope gradient (0.053), incision spacing could not be determined because only one incision was initiated. Despite these uncertainties, incision spacing tended to decrease with

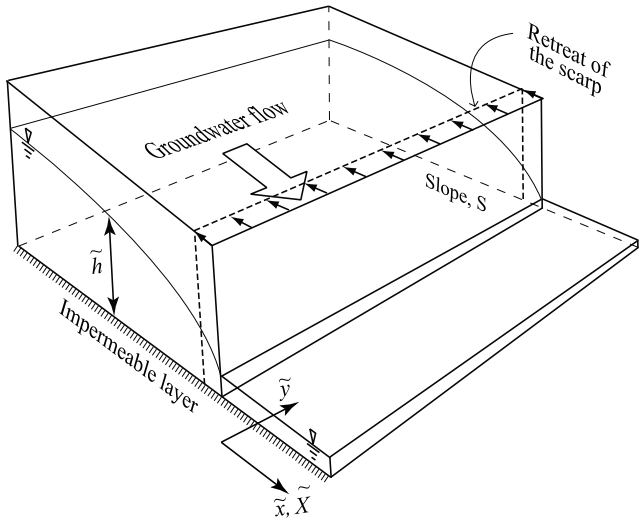

Figure 8. Conceptual diagram of a sediment layer with groundwater flow and a retreating scarp. The dashed line shows the uniformly retreating scarp.

an increase in slope for the 10 cm layer depth, but no clear relationship with slope was found for the 6 and 8 cm depths.

3. Theoretical Analysis

3.1. Groundwater Flow Equation

[17] Let us consider a three-dimensional seepage problem in an unconfined aquifer with a free water surface above an inclined impermeable layer (Figure 8). Following the models of landscape evolution by *Howard* [1988, 1995] and *Luo and Howard* [2008], groundwater flow can be described by the Dupuit-Forchheimer equation. Thus, the governing equation is

$$\frac{1}{\phi}\frac{\partial \tilde{h}}{\partial \tilde{t}} - \frac{\partial}{\partial \tilde{x}}\left[\tilde{K}\tilde{h}\left(\frac{\partial \tilde{h}}{\partial \tilde{x}} - S\right)\right] - \frac{\partial}{\partial \tilde{y}}\left(\tilde{K}\tilde{h}\frac{\partial \tilde{h}}{\partial \tilde{y}}\right) = 0 \qquad (1)$$

where $\tilde{}$ denotes the dimensional variables, $\tilde{t}$ is time, $\tilde{x}$ and $\tilde{y}$ are the longitudinal and lateral coordinates relative to the incision, respectively, $\tilde{h}$ is water depth, $\tilde{K}$ is the saturated hydraulic conductivity, ϕ is porosity, and S is the slope of an impermeable layer.

3.2. Retreat Rate of Scarp

[18] According to *Howard* [1995], many landforms exhibit distinct boundaries between dissimilar terrains and can be well characterized by the planimetric shape of the channel edge. Thus, models of scarp retreat have successfully represented various landscapes [*Howard*, 1988, 1995; *Flores-Cervantes et al.*, 2006]. In the case of seepage erosion, *Howard* [1995] postulated that the retreat rate of the scarp by seepage erosion and backwasting can be given by the relationship

$$\frac{\partial \tilde{n}}{\partial \tilde{t}} = \tilde{C}_s(\tilde{q} - \tilde{q}_{th})^{\gamma} + \tilde{C}_e \qquad (2)$$

where $\tilde{n}$ is the retreat distance in the direction normal to the scarp in the horizontal ($\tilde{x}$, $\tilde{y}$) plane, $\tilde{q}$ and $\tilde{q}_{th}$ are the unit discharge at the scarp and the threshold unit discharge for seepage erosion, respectively, and γ, $\tilde{C}_s$ and $\tilde{C}_e$ are empirical parameters.

[19] The first term on the right-hand side of (2) represents the retreat rate produced by seepage erosion. This can be expressed as a power law function of groundwater flow in excess of the threshold value. However, the second term ($\tilde{C}_e$), that reflects the effect of scarp backwasting, is difficult to estimate. Backwasting processes occur intermittently, and depend on material properties, geometry of the scarp, and hydraulic pressure [*Darby and Thorne*, 1996; *Istanbulluoglu et al.*, 2005]. Though *Howard* [1995] assumed that $\tilde{C}_e$ is a constant as a first approximation, he suggested that backwasting is enhanced by the convexity of the incision edge.

[20] It was hypothesized that the curvature of the incision edge affects the initiation of block failure (Figure 9). Three types of sediment blocks with the same volume but different shapes along the incision edge (concave, linear and convex shapes) were assumed to slide. Since the shape of each block differed, the corresponding failure surface area of each block differed. Under the condition that the blocks have the same volume, the failed surface area of the block reduces in size if the convexity of the incision edge increases. The resistance to block failure can be calculated by the sum of the friction stresses multiplied by the failure surface area. If the friction stress is independent of block shape, blocks with smaller failure surface areas (convex shapes) have higher possibilities of block failure. As previously indicated, tension cracks and mass failure often occur at pointed scarps, suggesting a high convexity of the incision edge. Therefore, upon mass failure, the overall planimetric shape of the incision edge became a concave shape.

[21] Although it is difficult to formulate the mass wasting process because it occurs intermittently and depends on several factors, it can be modeled as a continuous process if a sufficiently long time scale of development is employed. To model bed evolution, many researchers treat mass wasting as a diffusive-type process that depends on the curvature of hillslope [e.g., *Howard*, 1994; *Roering et al.*, 1999; *Kirkby and Bull*, 2000; *Kirkby et al.*, 2003]. However, in the case of planform evolution, no in-depth formulation of the mass wasting process has been proposed to the authors' knowledge. In this study, we hypothesized that the effect of the incision edge shape on the mass wasting

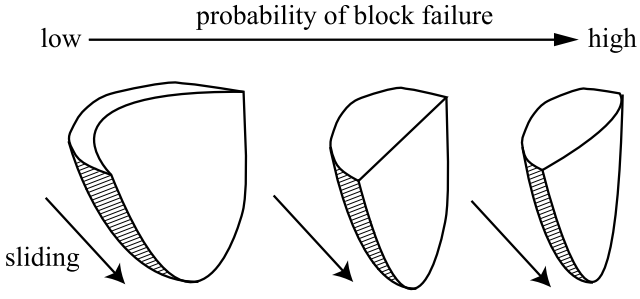

Figure 9. Hypothetical effect of the curvature of the incision edge on the probability of block failure. Sediment blocks with (left) concave, (middle) linear, and (right) convex shapes along the edges are shown. The shaded area shows the assumed failure surface.

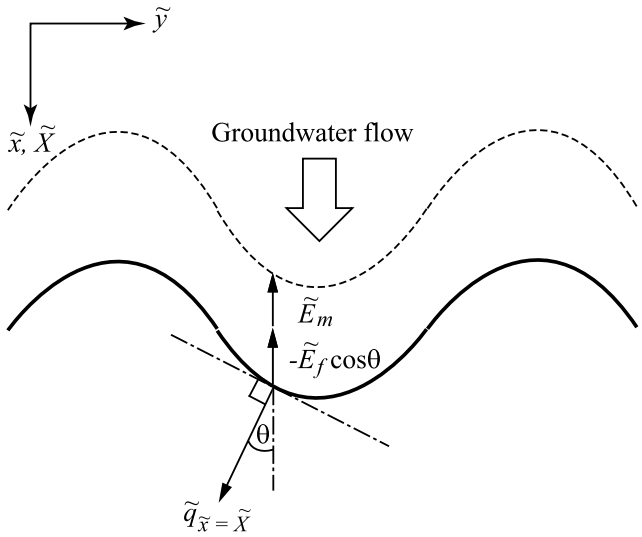

Figure 10. Schematic representation of the processes controlling the retreat of the scarp (seepage erosion and mass failure). The solid line is the initial incision edge, and the dashed line is the retreating incision edge.

process is one of the most important factors in the incision development. In the simplest description, the effect of the incision edge shape $\tilde{E}_m$ on retreat rate in the $\tilde{x}$ direction is assumed to be a diffusion-like function on the planimetric shape of the incision edge:

$$\tilde{E}_m = \tilde{\epsilon}\frac{\partial^2 \tilde{X}}{\partial \tilde{y}^2} \tag{3}$$

where $\tilde{\epsilon}$ denotes the diffusion-like coefficient influencing the magnitude of the retreat rate in the $\tilde{x}$ direction due to the incision edge shape, $\tilde{X}$ denotes the distance of the incision edge in the $\tilde{x}$ direction from the $\tilde{y}$ axis (Figure 10), and thus $\tilde{X}$ is a function of $\tilde{y}$ and $\tilde{t}$. It should be noted that from a mechanistic standpoint, $\tilde{E}_m$ is not simply defined as the retreat rate of the scarp due to the mass wasting process, but rather as the effect of the incision edge shape that may enhance or reduce the retreat rate of the scarp.

[22] The total retreat rate of the scarp in the $\tilde{x}$ direction is given by the relationship

$$\frac{\partial \tilde{X}}{\partial \tilde{t}} = -\tilde{E}_f \cos\theta + \tilde{E}_m \tag{4}$$

where $\tilde{E}_f$ is the retreat rate in the absence of the effect of the incision edge shape:

$$\tilde{E}_f = \begin{cases} \tilde{\alpha}\left(\dfrac{\tilde{q}_{\tilde{x}=\tilde{X}} - \tilde{q}_{th}}{\tilde{q}_r}\right)^{\gamma} & \text{if} \quad \tilde{q}_{\tilde{x}=\tilde{X}} \geq \tilde{q}_{th} \\ 0 & \text{if} \quad \tilde{q}_{\tilde{x}=\tilde{X}} < \tilde{q}_{th} \end{cases} \tag{5}$$

where $\tilde{q}_{\tilde{x}=\tilde{X}}$ and $\tilde{q}_r$ are the unit water discharge at the scarp ($\tilde{x} = \tilde{X}$) and the reference unit water discharge, respectively, $\tilde{\alpha}$ is an empirical constant with the dimension of velocity, and the exponent γ is between 1 and 1.6 according to the experiments conducted by *Fox et al.* [2006].

[23] As shown in Figure 10, θ is the angle between the direction normal to the incision edge and the $\tilde{x}$ axis. Thus

$$\cos\theta = \frac{1}{\sqrt{1 + \left(\partial \tilde{X}/\partial \tilde{y}\right)^2}} \tag{6}$$

and the unit water discharge $\tilde{q}$ can be computed by

$$\tilde{q} = \left(\tilde{u}^2 + \tilde{v}^2\right)^{1/2}\tilde{h} = \tilde{K}\left[\left(S - \frac{\partial \tilde{h}}{\partial \tilde{x}}\right)^2 + \left(-\frac{\partial \tilde{h}}{\partial \tilde{y}}\right)^2\right]^{1/2}\tilde{h} \tag{7}$$

where $\tilde{u}$ and $\tilde{v}$ are volume fluxes in the $\tilde{x}$ and $\tilde{y}$ directions, respectively.

[24] Models of long-term bed evolution (landscape evolution) commonly consist of advective erosion processes (e.g., stream incision) and diffusive transport processes (e.g., soil creep) [e.g., *Howard*, 1994; *Kooi and Beaumont*, 1996; *Densmore et al.*, 1998; *Tucker and Bras*, 1998]. While the advective processes generate incisions on the slope, the diffusive processes level out the slope. Recently, *Perron et al.* [2008, 2009] found that first-order valley spacing can be analyzed by process competition between the advective and diffusive processes. The present model of planform evolution by seepage and the long-term bed evolution models represent similar concepts of process competition, but use different governing equations and sediment transport process relationships. While the present model introduces the groundwater flow equation (1) and a formula on the planimetric retreat of the scarp (equation (4)), many other models employ the equation of the evolution of bed elevation. In addition, our model assumes that the advective term is a function of seepage flow (equation (5)), and the diffusive term depends on the shape of the incision edge as defined by (3) while many other models assume that the advective term depends on drainage area and hillslope gradient, and the diffusive term depends on hillslope curvature. A concept of process competition in our study is illustrated in Figure 11. Small sinusoidal perturbations with various wave numbers k were assumed to be imposed at the incision edge. In case a, the perturbation with a small wave number k (large incision spacing) is imposed on the incision edge (Figure 11a). Due to large incision spacings, the effect of the incision edge shape on mass wasting is small, and the retreat rate of the scarp in the vicinity of the incision head is higher than in other sections because of the amount of groundwater seepage. Thus, the perturbation will grow in time and develop into incisions. In contrast, the effect of the incision edge shape will increase if the wave number of perturbation k is high (small incision spacing) (Figure 11b). The retreat rate of the scarp in the vicinity of the perturbation head is smaller than in other portions because the high concavity of the incision head shape slows the retreat rate. Thus, the scarp does not undergo incision development due to perturbations with sufficiently high wave numbers k. By using this concept of process competition, we can investigate the characteristic incision spacing with a linear stability analysis.

3.3. Boundary Conditions

[25] Let us assume that the sediment layer extends from the scarp ($\tilde{x} = \tilde{X}$) far into the aquifer ($\tilde{x} \rightarrow -\infty$). Since the

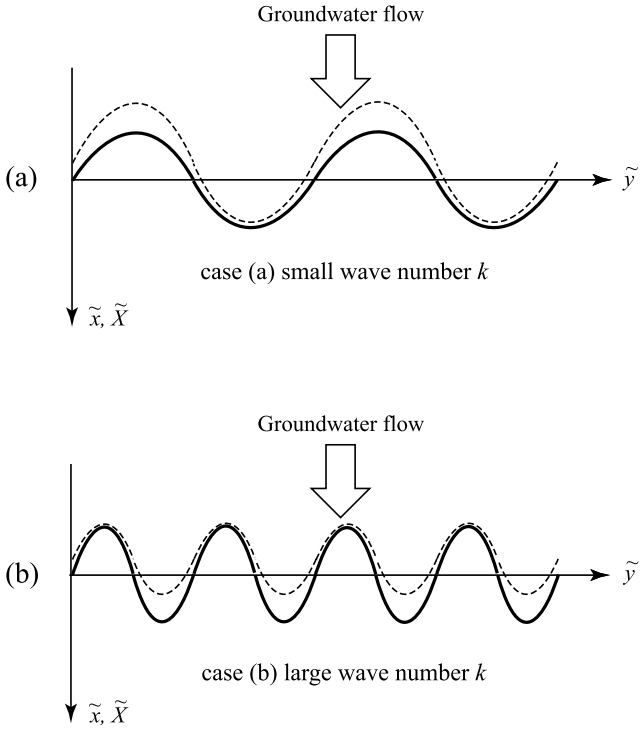

Figure 11. Concept of process competition. The retreat rate and incision development are affected by seepage flow (advective process) and the shape of the incision edge (diffusive process). The solid lines are the assumed initial perturbations, and the dashed lines are the evolutions of the perturbation. (a) Perturbation with small wave number k was imposed, and it can develop into incisions because the advective process dominated. (b) Perturbation with large wave number k was imposed, but it cannot develop into incisions because the diffusive process dominated.

impermeable slope S is assumed to be a constant, the seepage flow should be constant and a laterally uniform flow condition exists upstream from the seepage surface into the aquifer. Thus, we have

$$(\tilde{u}, \tilde{v}) = \left(\tilde{K}S, 0\right), \quad \tilde{h} = \tilde{H}_{-\infty} \quad \text{as} \quad \tilde{x} \to -\infty \tag{8}$$

where $\tilde{H}_{-\infty}$ denotes the constant groundwater depth far upstream in the aquifer.

[26] If there is no reservoir downstream from the scarp, the water depth will be nearly zero. If the water depth is zero, the velocity at the scarp, however, would be infinite based on the Dupuit approximation. Therefore, a nonzero value of water depth must be assumed at the scarp. Considering a constant water depth at the scarp ($\tilde{h}_\epsilon$), then the boundary condition at the scarp can be written as

$$\tilde{h} = \tilde{h}_\epsilon \quad \text{at} \quad \tilde{x} = \tilde{X} \tag{9}$$

3.4. Normalization

[27] The following normalizations are introduced, in which the variables without tildes are the normalized version of the corresponding variables with tildes:

$$\left(\tilde{x}, \tilde{y}, \tilde{X}\right) = \frac{\tilde{H}_{-\infty}}{S}(x, y, X), \tag{10a}$$

$$\tilde{h} = \tilde{H}_{-\infty} h, \tag{10b}$$

$$\tilde{t} = \frac{\tilde{H}_{-\infty}}{S\tilde{\alpha}} t, \tag{10c}$$

$$\tilde{q}_r = \tilde{K}S\tilde{H}_{-\infty} \tag{10d}$$

With the use of normalizations (10a)–(10d), the governing equations (1) and (4) can be rewritten as

$$\beta^{-1}\frac{\partial h}{\partial t} + \frac{\partial h}{\partial x} - \frac{\partial}{\partial x}\left(h\frac{\partial h}{\partial x}\right) - \frac{\partial}{\partial y}\left(h\frac{\partial h}{\partial y}\right) = 0 \tag{11}$$

$$\frac{\partial X}{\partial t} = -E\cos\theta + \epsilon\frac{\partial^2 X}{\partial y^2} \tag{12}$$

where the normalized seepage erosion function E is given by the relationships

$$E = \begin{cases} (q_{x=X} - \psi)^\gamma & \text{if} \quad q_{x=X} \geq \psi \\ 0 & \text{if} \quad q_{x=X} < \psi \end{cases} \tag{13}$$

Here, ψ denotes the ratio between the threshold discharge for seepage erosion and the reference water discharge; $q_{x=X}$ is the normalized unit discharge at the scarp that can be expressed as

$$q_{x=X} = \left\{\left(1 - \frac{\partial h}{\partial x}\right)^2 + \left(\frac{\partial h}{\partial y}\right)^2\right\}^{1/2} h \quad \text{at} \quad x = X \tag{14}$$

[28] In (11), parameter β indicates the relationship between groundwater flow velocity and seepage erosion as

$$\beta = \frac{\phi\tilde{K}S}{\tilde{\alpha}} \tag{15}$$

[29] In (12), the normalized diffusion-like coefficient ϵ denotes

$$\epsilon = \frac{\tilde{\epsilon}S}{\tilde{\alpha}\tilde{H}_{-\infty}} \tag{16}$$

[30] ψ is given by the relationship

$$\psi = \frac{\tilde{q}_{th}}{\tilde{K}S\tilde{H}_{-\infty}} \tag{17}$$

where $0 \leq \psi < 1$.

[31] The boundary conditions (8) and (9) are normalized as

$$h = 1 \quad \text{as} \quad x \to -\infty \tag{18}$$

$$h = h_\epsilon \quad \text{at} \quad x = X \tag{19}$$

where $0 < h_\epsilon < 1$.

3.5. Coordinate Transformation

[32] If one considers the base state of the problem in which the scarp retreats at a constant rate, then the variables such as water depth and velocity can be considered steady under appropriate moving coordinates. The following moving coordinates are introduced for convenience:

$$t^* = t, \tag{20a}$$

$$x^* = x - X_0 \tag{20b}$$

where $*$ denotes the moving coordinates, and X_0 is the location of the scarp in the base state and is a function of time t.

[33] From (20a) and (20b), the following relations are derived:

$$\frac{\partial}{\partial t} = \frac{\partial t^*}{\partial t}\frac{\partial}{\partial t^*} + \frac{\partial x^*}{\partial t}\frac{\partial}{\partial x^*} = \frac{\partial}{\partial t^*} - \frac{\mathrm{d}X_0}{\mathrm{d}t}\frac{\partial}{\partial x^*} \tag{21a}$$

$$\frac{\partial}{\partial x} = \frac{\partial t^*}{\partial x}\frac{\partial}{\partial t^*} + \frac{\partial x^*}{\partial x}\frac{\partial}{\partial x^*} = \frac{\partial}{\partial x^*} \tag{21b}$$

[34] Substitution of (21a) and (21b) into (11) and (12) yields

$$\beta^{-1}\frac{\partial h}{\partial t} + (f+1)\frac{\partial h}{\partial x} - \frac{\partial}{\partial x}\left(h\frac{\partial h}{\partial x}\right) - \frac{\partial}{\partial y}\left(h\frac{\partial h}{\partial y}\right) = 0 \tag{22}$$

$$\frac{\partial X}{\partial t} = -E\cos\theta + \epsilon\frac{\partial^2 X}{\partial y^2} \tag{23}$$

[35] For simplicity, $*$ has been dropped in (22) and (23), and will be dropped hereafter. The secondary parameter f in (22) denotes

$$f = -\beta^{-1}\frac{\mathrm{d}X_0}{\mathrm{d}t} \tag{24}$$

where $\mathrm{d}X_0/\mathrm{d}t$ is a constant retreat rate of the seepage face due to erosion for the base state.

3.6. One-Dimensional Base State

[36] In the one-dimensional base state, the flow is assumed to be uniform in the lateral direction (y direction); thus, the terms associated with the lateral direction are dropped. In addition, it is assumed that the base state of the groundwater surface profile does not change with time in a steady state flow regime in the moving coordinate system. Thus, the governing equation (22) can be reduced to

$$(f+1)\frac{\mathrm{d}h_0}{\mathrm{d}x} - \frac{\mathrm{d}}{\mathrm{d}x}\left(h_0\frac{\mathrm{d}h_0}{\mathrm{d}x}\right) = 0 \tag{25}$$

Using (23), the constant retreat rate of the seepage surface in the base state can be determined as follows:

$$\frac{\mathrm{d}X_0}{\mathrm{d}t} = -E_0, \quad E_0 = \left[\left(1 - \frac{\mathrm{d}h_0}{\mathrm{d}x}\right)h_0 - \psi\right]^{\gamma} \quad \text{at} \quad x = 0 \tag{26}$$

where subscript 0 denotes the one-dimensional base state solution, and $x = 0$ at the scarp.

[37] Integrating (25), we obtain

$$h_0 - \frac{h_0}{f+1}\frac{\mathrm{d}h_0}{\mathrm{d}x} + C_1 = 0 \tag{27}$$

Far upstream, $h_0 \to 1$ and $\mathrm{d}h_0/\mathrm{d}x \to 0$ as expressed in (18). Thus, we obtain $C_1 = -1$, and (27) becomes

$$\frac{\mathrm{d}h_0}{\mathrm{d}x} = -(f+1)\frac{1-h_0}{h_0} \tag{28}$$

[38] Again, integrating (28) and using the boundary condition (19), in which $h_0 = h_\epsilon$ at the scarp $x = 0$, we obtain

$$(h_0 - h_\epsilon) + \ln\left(\frac{1-h_0}{1-h_\epsilon}\right) - (f+1)x = 0 \tag{29}$$

where $h_\epsilon \le h_0 \le 1$, and the relation between x and h_0 is described by

$$x = \frac{1}{f+1}\left[(h_0 - h_\epsilon) + \ln\left(\frac{1-h_0}{1-h_\epsilon}\right)\right] \tag{30}$$

[39] Upon substitution of (24) and (28) into (26), the relationship amongst parameters h_ϵ, β, ψ, γ and f can be given by

$$h_\epsilon = 1 - \frac{(\beta f)^{1/\gamma} + \psi - 1}{f} \tag{31}$$

3.7. One-Dimensional Base State Solutions

[40] Using (30) and (31), all h_0 profiles have drawdown shapes from $h_0 \to 1$ far upstream ($x \to -\infty$) to $h_0 = h_\epsilon$ at the scarp ($x = 0$) (Figure 12). The h_0 profile increases with an increase in the normalized downstream water depth h_ϵ (Figure 12a). If β (ratio between groundwater velocity and seepage erosion) increases to be an infinitely large value, f defined by (24) becomes approximately zero, and the h_0 profile approaches a specific profile (Figure 12b). A very large value of β implies that the retreat rate of the scarp is much slower than the groundwater flow velocity. Thus, the effect of the moving coordinates (f) decreases, and the h_0 profile in the moving coordinates becomes the same as the h_0 profile in the stationary coordinates.

3.8. Two-Dimensional Perturbation Problem

[41] We introduce expansions of the form

$$(X, h) = (X_0(t), h_0(x)) + A(X_1, h_1(x))\mathrm{e}^{\Omega t}\cos ky \tag{32}$$

where the subscript 1 denotes a linear solution, A is a small amplitude, Ω is the growth rate of perturbation, k is the wave number of perturbation, X_1 is a constant, and h_1 is a function of x. Substitution of (32) into (22) and (23) and expansion yields the following results. At the zero-power order of A, which is denoted by $O(1)$, (25) and (26) are exactly recov-

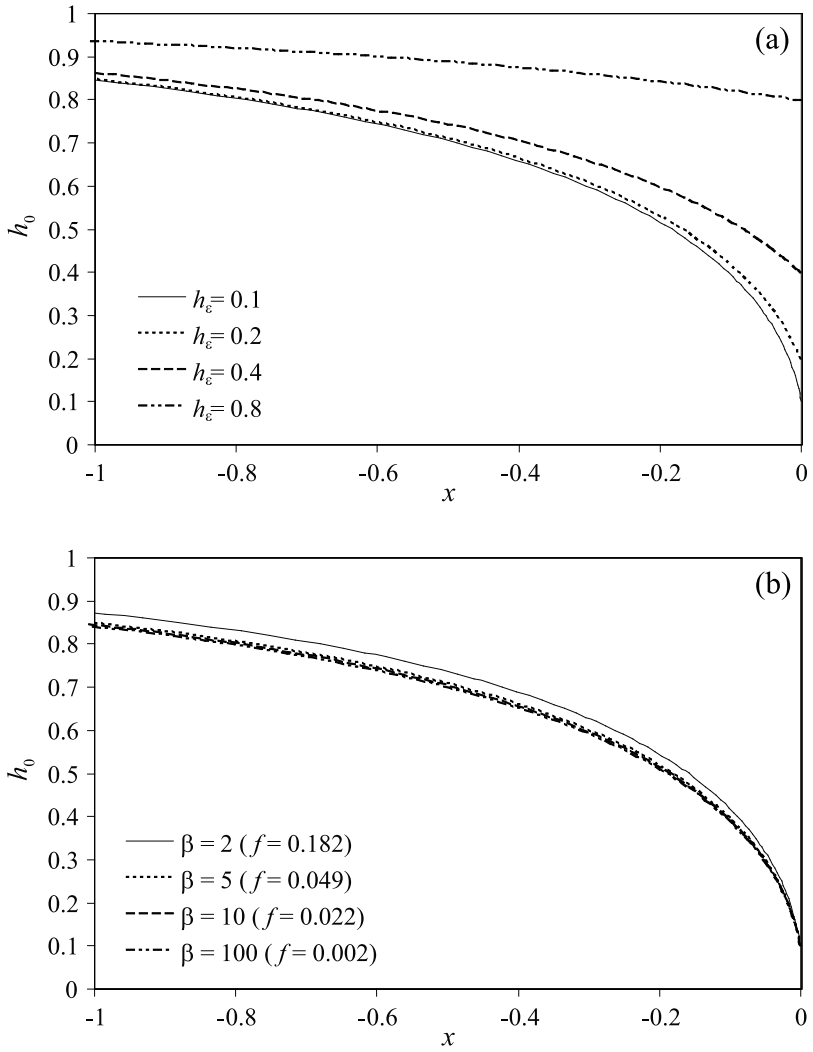

Figure 12. Normalized, base state water depth h_0 profiles. (a) The effect of the normalized downstream water depth h_ϵ while other parameters are constant ($\beta = 10$, $\psi = 0.8$, and $\gamma = 1$). (b) The effect of the scarp retreat by parameter β (the relationship between the groundwater velocity and the retreat rate) while other parameters are constant ($h_\epsilon = 0.1$, $\psi = 0.8$, and $\gamma = 1$).

ered. At the first power order of A, which is denoted by $O(A)$, we have

$$-h_0 h_1'' + (f + 1 - 2h_0')h_1' + \left(\beta^{-1}\Omega + k^2 h_0 - h_0''\right)h_1 = 0 \quad (33)$$

$$\Omega X_1 + \gamma E_0^{1-1/\gamma}(1 - h_0')h_1 - \gamma E_0^{1-1/\gamma} h_0 h_1' + k^2 \epsilon X_1 = 0 \quad \text{at} \quad x = 0 \quad (34)$$

where $'$ denotes the derivative with respect to x. The perturbation equation (33) forms a second-order ordinary differential equation with an eigenvalue Ω.

[42] Far upstream from the scarp, the water depth asymptotically approaches a constant as shown in (18), and the perturbation should disappear such that

$$h_1 = 0 \quad \text{as} \quad x \to -\infty \quad (35)$$

[43] At the downstream end where the scarp is located, the boundary condition (19) becomes

$$h_1 + h_0' X_1 = 0 \quad \text{at} \quad x = 0 \quad (36)$$

[44] Eliminating X_1 by substituting (34) into (36) and further simplification, we obtain the second boundary condition as follows:

$$\left(\frac{\Omega + k^2\epsilon}{h_0'} - \gamma E_0^{1-1/\gamma}(1 - h_0')\right)h_1 + \gamma E_0^{1-1/\gamma} h_0 h_1' = 0 \quad \text{at} \quad x = 0 \quad (37)$$

[45] The governing equation (33) with the boundary conditions (35) and (37) will be solved for the eigenvalue Ω by the use of the spectral collocation method incorporated with the Chebyshev polynomials [*Boyd*, 2001].

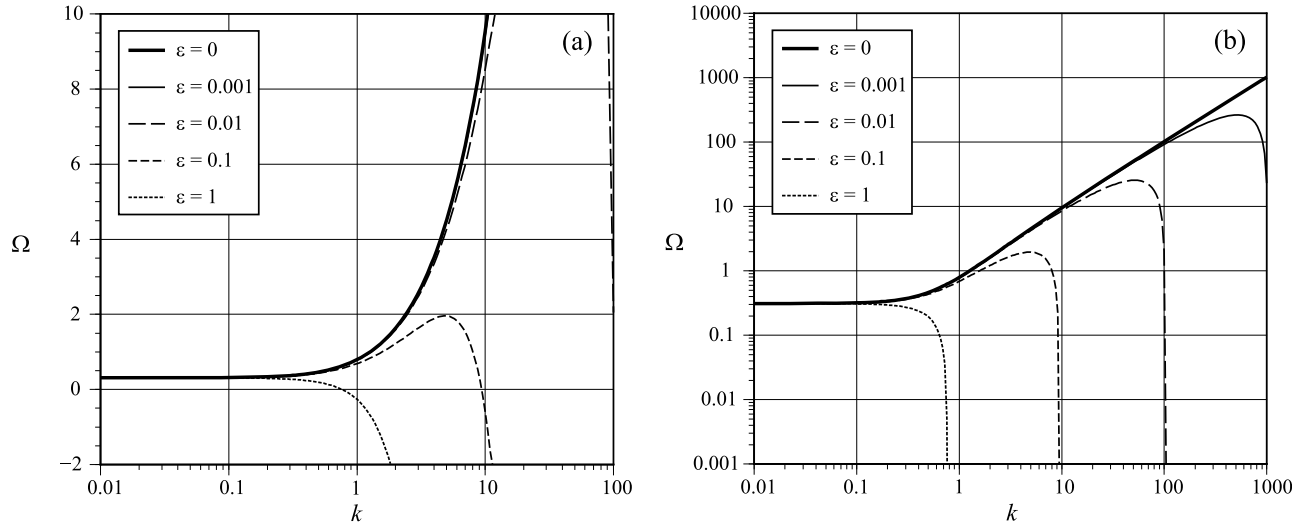

Figure 13. Growth rate of perturbation Ω as a function of k and ϵ for $\beta = 10$, $\gamma = 1.5$, and $h_\epsilon = 0.4$. (a) Ω is plotted on a linear scale, and (b) Ω is plotted on a logarithmic scale.

3.9. Results and Discussion of Stability Analysis

[46] The characteristics of the growth rate of the perturbation Ω as a function of the wave numbers k and the parameter ϵ that indicates the influence of the incision edge shape on the retreat rate of the scarp are shown in Figure 13. While k is presented in a logarithmic scale, Ω is shown in both a linear scale (Figure 13a) and a logarithmic scale (Figure 13b). When $\epsilon = 0$, the retreat rate of the scarp will depend on water discharge only. In that case (see Figure 13b), Ω increases linearly with increasing k, and no characteristic incision spacing was found. *Howard* [1988] discovered this shortcoming in his numerical model and resolved the problem by imposing a random function on the hydraulic conductivity K. However, the incision spacing in his model depended on the numerical grid size and the nature of the random function selected. Applying a nonzero value to ϵ, the retreat rate of the scarp will also depend on its shape. For a sufficiently small range of k, Ω does not change, but for larger k values, Ω shows a sharp decrease. Thus, the dominant wave numbers of perturbations $k_{\max}$ that correspond to the maximum growth rates of perturbations $\Omega_{\max}$ can be estimated. For $\epsilon = 0.001$, 0.01 and 0.1, $k_{\max}$ values are approximately 500, 50, and 5, respectively (Figure 13). Thus, the effect of the incision edge shapes places constraints on the incision frequency for sufficiently large k values (small incision spacing), and $k_{\max}$ decreases with an increase in ϵ. However, $k_{\max}$ becomes infinitely small when ϵ approaches unity.

[47] Thus, it is evident that the characteristic incipient incision spacing cannot be obtained when the diffusive process is excluded (Figure 13). In this study, the mass wasting process is formulated as a diffusive process from a physical consideration. It should be noted, however, that in linear stability analyses of incision development by overland flow [*Izumi and Parker*, 2000; *Izumi and Fujii*, 2006; *Pornprommin et al.*, 2009], the diffusive process is unnecessary. The characteristic incipient incision spacing can be derived by the shallow water flow equations and the bed evolution model in which the erosional process relates to flow velocity alone. However, the estimation of the diffusion-like coefficient $\tilde{\epsilon}$ is critical in the present analysis of incision development by seepage erosion. This will be discussed in the next section.

[48] In Figure 14a, β represents the relationship between groundwater velocity and the retreat rate of the scarp. When β is small, the seepage erosion is strong and comparable to the groundwater velocity. We found that the growth rate of perturbation Ω and the dominant wave number $k_{\max}$ increase with a decrease in β. In addition, β affects Ω for a wide range of small and moderate k values (moderate and large incision spacing).

[49] Values of Ω and $k_{\max}$ increase with an increase in the exponent of the erosion rate function γ (Figure 14b). Although γ exhibits a similar effect as β, the increase in Ω concentrates with a moderate range of k values. This implies that with an increase in γ, a clear characteristic incision spacing can be easily determined.

[50] In Figure 14c, h_ϵ is the ratio of water depth at the scarp $\tilde{h}_\epsilon$ to groundwater depth far upstream ($\tilde{H}_{-\infty}$). Both Ω and $k_{\max}$ increase with a decrease in h_ϵ. A decrease in h_ϵ implies that there is an increase in the difference in water depths between the scarp and far upstream, and thus the gradient of the piezometric head steepens in the vicinity of the scarp. The large gradient of the piezometric head causes the groundwater flow to increase, which corresponds to an increase in Ω. The effect of h_ϵ (Figure 14c) is similar to that of β (Figure 14a) in the sense that the growth rate of perturbation Ω increases with decreasing either h_ϵ or β in a wide range of small and moderate wave numbers k.

[51] The effect of ψ, the ratio of the threshold water discharge for seepage erosion ($\tilde{q}_{th}$) relative to the base state water discharge ($\tilde{q}_r$), is shown in Figure 14d. Both Ω and $k_{\max}$ increase with decreasing ψ. Thus, incisions with small spacings develop when water discharge is well above the threshold value for erosion. *Howard* [1988] conducted seepage erosion experiments for cases where water discharge was both slightly above and well above the erosion threshold, and found that more incisions initiated when discharge was well above the threshold because the competition between adjacent incisions is less pronounced. The

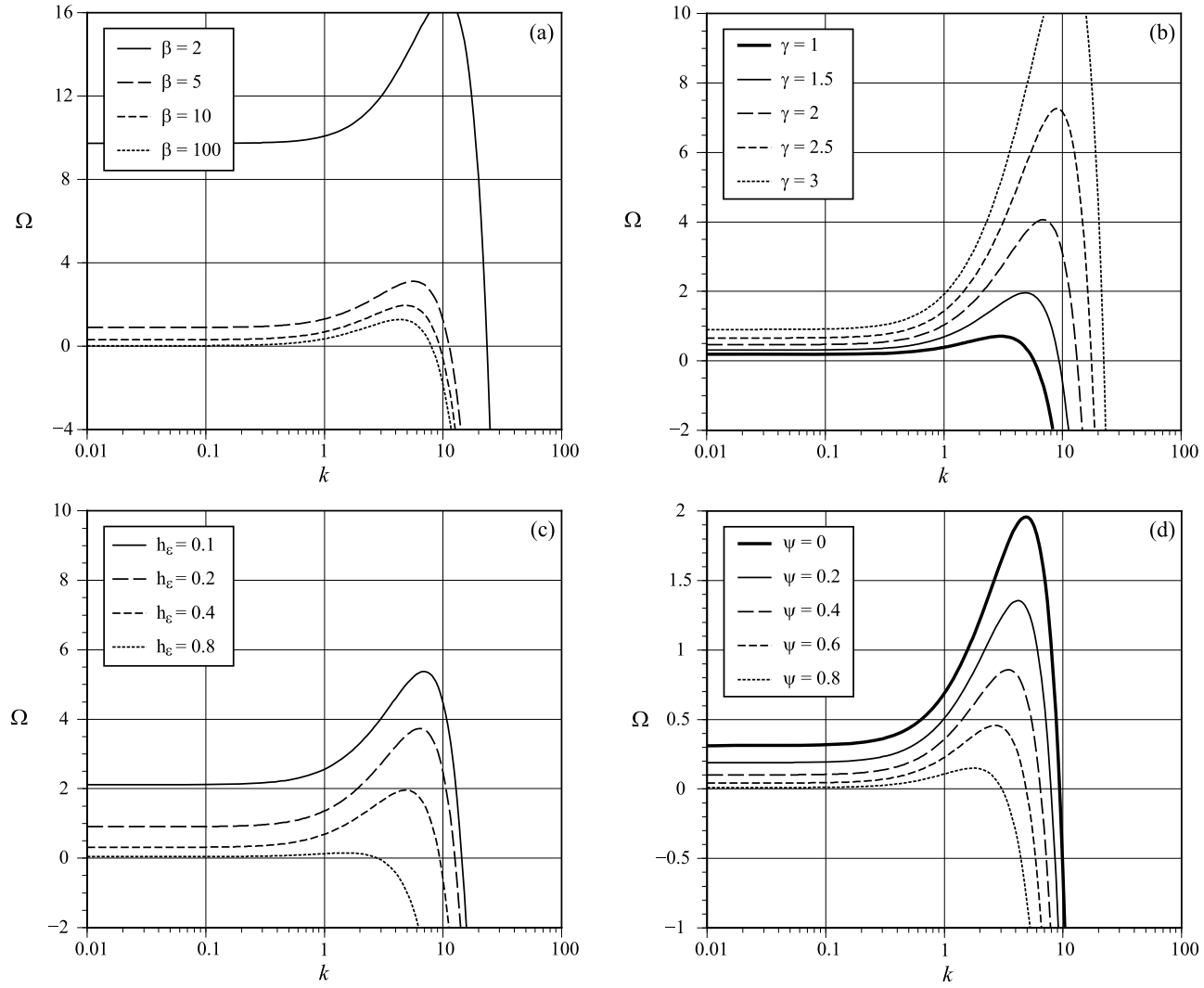

Figure 14. Growth rates of perturbation Ω as a function of k and (a) β for $\epsilon = 0.1$, $\gamma = 1.5$, and $h_\epsilon = 0.4$; (b) γ for $\epsilon = 0.1$, $\beta = 10$, and $h_\epsilon = 0.4$; (c) h_ϵ for $\epsilon = 0.1$, $\beta = 10$, and $\gamma = 1.5$; and (d) ψ for $\epsilon = 0.1$, $\beta = 10$, $\gamma = 1.5$, and $h_\epsilon = 0.4$.

present analysis agrees with the results of *Howard*'s [1988] experiments. In addition, the effect of ψ (Figure 14d) was similar to the effect of γ (Figure 14b) in which an increase in Ω is concentrated in a moderate range of k values.

3.10. Estimation of the Diffusion-Like Coefficient $\tilde{\epsilon}$

[52] In the previous section, the analysis showed that with proper treatment of the diffusion-like coefficient $\tilde{\epsilon}$, the characteristic incision spacing can be generated, and the model can operate independently of random functions imposed on the hydraulic conductivity and grid size. Although the highly complex nature of the mechanisms of the three-dimensional slope failure by seepage erosion makes it quite difficult to estimate $\tilde{\epsilon}$, our limited experimental data are still useful.

[53] Estimates of the diffusion-like coefficient $\tilde{\epsilon}$ derived from our experiments are shown in Table 2. From these measurements, the porosity ϕ and the hydraulic conductivity $\tilde{K}$ of the sediment layer are approximately 0.3 and 10 cm/s, respectively. As described in Section 2.2.3, incision spacing can be estimated only when more than one incision appears in the experiments. This requirement was met in 17 of the 27 experiments. The first four columns of Table 2 show the conditions and results of the experiment: the depth of the sediment layer $\tilde{D}$, the chamber slope S, the unit water discharge $\tilde{q}_r$ and the incision spacing $\tilde{L}$. The normalized water depth at the scarp h_ϵ in the fifth column is computed by $\tilde{h}_\epsilon/\tilde{H}_{-\infty}$, where the water depth at the scarp $\tilde{h}_\epsilon$ is assumed to be equal to the Froude critical water depth, since the scarp is located on the downstream side of the apparatus chamber, and the water depth far upstream ($\tilde{H}_{-\infty}$) is calculated by using (10d). Then, the normalized wave number k_{exp} that corresponds to the experimental incision spacing $\tilde{L}$ in the sixth column can be computed by

$$k_{\text{exp}} = \frac{2\pi\tilde{H}_{-\infty}}{S\tilde{L}} \tag{38}$$

[54] Values of k_{exp} decrease with increasing S because it is normalized with $\tilde{H}_{-\infty}/S$ (Table 2). To compute β, which

Table 2. Estimation of the Diffusion-Like Coefficient $\tilde{\epsilon}$ by Using the Experimental Results

Layer Depth $\tilde{D}$ (cm)	Chamber Slope S	Water Discharge $\tilde{q}_r$ (L/min)	Incision Spacing $\tilde{L}$ (cm)	h_ϵ	$k_{\exp}$	β	ϵ	$\tilde{\epsilon}$ (cm^2/s)	$\Delta\tilde{h}\tilde{F}_g^{1/2}$ (cm^2/s)
10	0.107	16.5	59.1	0.09	1.69	3.9	0.19	0.25	46.9
10	0.161	15.0	42.4	0.14	0.95	5.8	0.28	0.15	32.4
10	0.214	21.5	39.3	0.16	0.83	7.7	0.30	0.13	39.0
10	0.266	20.7	39.4	0.20	0.52	9.6	0.37	0.10	31.7
10	0.266	19.8	34.9	0.21	0.56	9.6	0.36	0.09	30.2
10	0.317	18.5	34.2	0.25	0.38	11.4	0.40	0.07	24.2
10	0.317	21.4	44.0	0.24	0.34	11.4	0.41	0.08	28.5
10	0.367	14.5	34.7	0.32	0.22	13.2	0.42	0.04	15.9
8	0.161	16.3	87.2	0.13	0.50	5.8	0.37	0.21	31.7
8	0.266	21.1	38.1	0.20	0.55	9.6	0.36	0.10	29.0
8	0.317	19.2	84.1	0.25	0.16	11.4	0.45	0.08	22.6
8	0.367	19.8	36.4	0.28	0.28	13.2	0.41	0.06	20.3
6	0.161	21.1	70.4	0.12	0.81	5.8	0.31	0.23	36.6
6	0.214	20.9	59.6	0.16	0.54	7.7	0.37	0.16	29.5
6	0.266	21.7	82.3	0.20	0.26	9.6	0.44	0.12	25.9
6	0.317	22.0	75.1	0.24	0.20	11.4	0.45	0.09	22.7
6	0.367	21.2	41.1	0.28	0.27	13.2	0.42	0.06	19.0

represents the relationship between the groundwater velocity and retreat rate of the scarp, we use the definition of β in (15). To this end, it is necessary to estimate the coefficient $\tilde{\alpha}$ in the retreat rate function $\tilde{E}_f$ defined in (5). From the results of these experiments, the initial $\tilde{E}_f$ is roughly on the order of 1 cm/min, but this increases as the scarp retreat induces groundwater flow concentration. As a first approximation, we assigned a constant value of 1 cm/min to $\tilde{E}_f$. Since the experiments were conducted under the assumption that water discharge will increase slightly until it initiates incision, the discharge ($\tilde{q}_r$) should be just above the erosion threshold. Thus, ψ, which is the ratio between the threshold water discharge for seepage erosion and base state water discharge ($\tilde{q}_{th}/\tilde{q}_r$), is assumed to be 0.8. According to the results of the two-dimensional seepage erosion experiments by *Fox et al.* [2006], the exponent of the erosion rate function γ is between 1 and 1.6. In this analysis, γ is assumed to be unity. Thus, $\tilde{\alpha}$ in (5) and β in (15) can be estimated with the use of $\tilde{E}_f$, ψ and γ. The values of β increases with an increase in S (Table 2, seventh column).

[55] With the use of h_ϵ, ψ, γ and β, the normalized diffusion-like coefficient ϵ (Table 2, eighth column) is chosen under the condition that the wave number $k_{\exp}$ in the experiment is equal to the dominant wave number $k_{\max}$ corresponding to the maximum growth rate $\Omega_{\max}$ analyzed in the linear stability analysis. We established that ϵ has the value in the order of 0.1. We recalculated the analysis for some uncertain assumptions, such as $\tilde{E}_f$ and γ, and found that the value of ϵ does not change to any great degree. Finally, the dimensional diffusion-like coefficient $\tilde{\epsilon}$ (Table 2, ninth column) is then calculated by using (16).

[56] At this stage, we attempt to estimate $\tilde{\epsilon}$ with the use of some parameters controlling the mechanisms of slope instability. Since $\tilde{\epsilon}$ has the dimension of length^2/time, the combination of the parameters should have the same dimensions. The driving forces, hydraulic pressure and the weight of a failure block along a failure plane, are important factors in the slope stability analysis. Thus, these were selected as the parameters to be used in our preliminary investigation. However, this does not imply that $\tilde{\epsilon}$ can be satisfactorily estimated with the use of these parameters alone. Our purpose is to show that $\tilde{\epsilon}$ can be related to the mechanisms of slope instability. Let us consider the following combination of the driving forces:

$$\Delta\tilde{h}\tilde{F}_{\mathrm{g}}^{1/2} = \left(\tilde{H}_{-\infty} - \tilde{h}_\epsilon\right) \cdot \sqrt{\mathrm{g}\left\{\mathrm{SG}\left(\tilde{D} - \tilde{h}_\epsilon\right)(1-\phi) + \left(\tilde{H}_{-\infty} - \tilde{h}_\epsilon\right)\phi\right\}\sin\theta_2} \tag{39}$$

where $\Delta\tilde{h}$ denotes the difference in water depths far upstream and at the scarp, $\tilde{F}_g$ denotes the driving force by the gravity with the assumption that the failure plane is parallel to the chamber slope, g is the gravitational acceleration, SG denotes the specific gravity of sediment, and θ_2 is the angle of the sediment chamber.

[57] The value of $\tilde{\epsilon}$ increases with an increase in $\Delta\tilde{h}\tilde{F}_{\mathrm{g}}^{1/2}$ (Figure 15), and this relationship ($R^2 = 0.6$) can be quantified as

$$\tilde{\epsilon} = 0.0043\Delta\tilde{h}\tilde{F}_{\mathrm{g}}^{1/2} \tag{40}$$

[58] Thus, as the first step for estimating the diffusion-like coefficient $\tilde{\epsilon}$, which represents the effect of the incision edge shape on the retreat rate, we found that driving force is an important parameter. However, we recommend that other factors such as sediment properties and the resistant forces should be considered in future studies.

4. Conclusion

[59] The experimental study and the theoretical analysis were conducted in order to investigate the characteristics of incision development and growth brought about by seepage erosion. In the experiments, sediment layers with dimensions of 1.50 m in width, 1.20 m in length and varying depths of 6, 8 and 10 cm were constructed with coarse plastic pellets as sediment. The chamber slope gradient was also varied to investigate the effect of the two-layer alignment of the sediment layer and an impermeable layer. The results of the experiment reveal that under similar water discharges, a steeper chamber slope causes a shallower

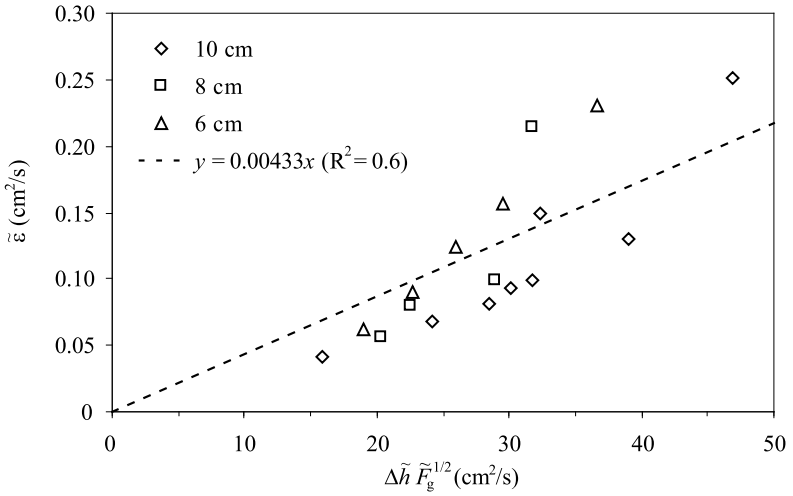

Figure 15. Relationship between the combination of driving forces $\Delta\tilde{h}\tilde{F}_g^{1/2}$ in the slope stability analysis and the diffusion-like coefficient $\tilde{\epsilon}$.

water depth, sediment emergence in the incised area and a lowering of the difference in water depths between the upstream end and the scarp. Sediment emergence in the incised area reduces the capacity of fluvial transport [*Lamb et al.*, 2008], and therefore retards the erosion. The lowering of the difference in the water depths weakens flow concentration and results in an increase in the number of incisions. As the depth of the sediment layer increases, the incision width also increased. It is possible that an increase in depth causes mass failure at a large scale and this results in wider incisions. Moreover, we found that water discharge that initiates an incision increases with a decrease in the depth of the sediment layer. This may be due to the fact that slope stability increases with a decrease in the height of a scarp. It has been established that incision development can be significantly affected by water discharge and types of sediment [*Howard*, 1988]. This study shows that the formation and evolution of incisions is also influenced by the chamber slope and the sediment layer depth.

[60] In the theoretical study, we performed a linear stability analysis to investigate the inception of incisions by seepage erosion. The characteristic incision spacing is derived from the wavelength associated with the maximum growth rate of perturbation in the linear stability analysis. Since many landforms can be characterized by a planimetric shape of the channel edge, the present analysis investigated incision development by planform morphology. The Dupuit-Forchheimer equation was used as the groundwater flow model, and the equation describing the retreat of the scarp was employed as a landform evolution model. The retreat rate of the scarp was assumed to consist of two terms that express two processes: seepage erosion and mass failure. The first term is a power law function of the specific discharge at the scarp exceeding a threshold discharge for erosion. The second term, a diffusion-like function of the incision edge shape, is hypothesized in order to estimate the effect of the incision edge shape on mass wasting and the retreat rate of the scarp. If the edge shape is convex, the mass wasting process should be enhanced, and thus the retreat rate of the scarp increases. On the other hand, a concave edge shape may retard the mass wasting process and the retreat rate. Excluding the second term, we found that the growth rate of perturbation increases linearly with an increase in the wave number of perturbation, which implies that the characteristic incision spacing is infinitely small. This shortcoming found, by *Howard* [1988] in his numerical simulation, was theoretically confirmed in this study. As the diffusion-like coefficient in the second term increases, the characteristic incision spacing increased. In addition, the analysis found that the incision spacing decreases where the seepage erosion becomes stronger, e.g., where water discharge is well above the threshold value, or where the retreat rate of the scarp is comparable with the groundwater velocity. Finally, as an initial step for estimating the diffusion-like coefficient, using the results of the experiment on incision spacing, we discovered a linear relationship between the diffusion-like coefficient and the combination of driving forces, hydraulic pressure and the component of failure block weight along a failure plane.

Notation

A small amplitude of perturbations.
$\tilde{C}_s$, $\tilde{C}_e$ parameters in (2).
$\tilde{D}$ sediment layer depth.
E normalized seepage erosion function.
$\tilde{E}_f$ retreat speed (not considering the effect of the incision edge shape).
$\tilde{E}_m$ effect of the incision edge shape on the retreat speed of the scarp.
$\tilde{F}_g$ driving force by gravity.
f secondary parameter indicating the effect of the retreat of the scarp on the base state solutions.
g gravitational acceleration.
$\tilde{H}_{-\infty}$ constant water depth far upstream.
$\tilde{h}$, h water depth and normalized water depth.
$\tilde{h}_\epsilon$, h_ϵ constant water depth at the scarp and normalized constant water depth at the scarp.
$\Delta\tilde{h}$ difference in water depths far upstream and at the scarp.
$\tilde{K}$ hydraulic conductivity.

k wave number of perturbation.
k_{exp} wave number corresponding to the incision spacing in the experiment.
k_{max} dominant wave number corresponding to Ω_{max}.
$\tilde{L}$ incision spacing.
$\tilde{n}$ retreat distance in the direction normal to the incision edge in the horizontal ($\tilde{x}$, $\tilde{y}$) plane in (2).
$\tilde{q}$, $\tilde{q}_r$, $\tilde{q}_{th}$ unit discharge, reference unit discharge and threshold unit discharge for seepage erosion.
$\tilde{q}_{\tilde{x}=\tilde{X}}$, $q_{x=X}$ unit water discharge at the scarp and normalized unit water discharge at the scarp.
S slope of the impermeable layer.
SG specific gravity of sediment.
$\tilde{t}$, t time and normalized time.
$\tilde{u}$, $\tilde{v}$ volume fluxes in the $\tilde{x}$ and $\tilde{y}$ directions.
$\tilde{X}$, X distance of the scarp in the $\tilde{x}$ direction from the $\tilde{y}$ axis and normalized distance of the scarp.
$\tilde{x}$, $\tilde{y}$ longitudinal and lateral directions.
x, y normalized longitudinal and lateral directions.
$\tilde{\alpha}$ empirical constant with the dimension of velocity in retreat speed function.
β parameter representing the relationship between groundwater flow velocity and seepage erosion.
γ exponent of the retreat speed function.
$\tilde{\epsilon}$, ϵ diffusion-like coefficient influencing the magnitude of the retreat speed due to the incision edge shape and normalized diffusion-like coefficient.
θ angle between the direction normal to the incision edge and the $\tilde{x}$ axis.
θ_2 angle of chamber.
ϕ porosity.
ψ ratio between the threshold water discharge for seepage erosion and the reference water discharge.
Ω growth rate of perturbation.
Ω_{max} maximum growth rate.
$\tilde{()}$ dimensional variables.
$()'$ derivative with respect to x.
$()_0$ base state solutions.
$()_1$ linear solutions.
$*$ moving coordinates.

[61] **Acknowledgments.** This work was supported by the Hokkaido River Disaster Prevention Research Center and the Japan Society for the Promotion of Science Postdoctoral Fellowship Program (grant-in-aid P 07116). We gratefully acknowledge Roy C. Sidle and the four anonymous reviewers for their constructive comments and editorial corrections of our manuscript.

References

Abam, T. K. S. (1993), Factors affecting distribution of instability of river banks in the Niger delta, *Eng. Geol.*, *35*, 123–133.

Boyd, J. P. (2001), *Chebyshev and Fourier Spectral Methods*, 2nd ed., Dover, Mineola, N. Y.

Bradford, J. M., and R. F. Piest (1980), Erosional development of valley-bottom gullies in the upper midwestern United States, in *Thresholds in Geomorphology*, edited by D. R. Coates and J. D. Vitek, pp. 75–101, Allen and Unwin, St. Leonards, NSW, Australia.

Bull, L. J., and M. J. Kirkby (1997), Gully processes and modelling, *Prog. Phys. Geogr.*, *21*, 354–374.

Carey, B. (2006), Gully erosion, in *Fact Sheets: Land Series*, *Rep. L81*, Dep. of Nat. Resour. and Water, Qld. Gov., Brisbane, Qld., Australia. (Available at http://www.nrw.qld.gov.au/factsheets/pdf/land/l81.pdf.)

Chu-Agor, M., G. A. Fox, R. M. Cancienne, and G. V. Wilson (2008a), Seepage caused tension failures and erosion undercutting of hillslopes, *J. Hydrol.*, *359*, 247–259, doi:10.1016/j.jhydrol.2008.07.005.

Chu-Agor, M., G. V. Wilson, and G. A. Fox (2008b), Numerical modeling of bank instability by seepage erosion undercutting of layered streambanks, *J. Hydrol. Eng.*, *13*(12), 1133–1145.

Darby, S. E., and C. R. Thorne (1996), Development and testing of riverbank-stability analysis, *J. Hydraul. Eng.*, *122*, 443–454.

Densmore, A. L., M. A. Ellis, and R. S. Anderson (1998), Landsliding and the evolution of normal-fault-bounded mountains, *J. Geophys. Res.*, *103* (B7), 15,203–15,219.

Dietrich, W. E., and T. Dunne (1993), The channel head, in *Channel Network Hydrology*, edited by K. Beven and M. J. Kirkby, pp. 175–219, John Wiley, Hoboken, N. J.

Dunne, T. (1980), Formation and controls on channel networks, *Prog. Phys. Geogr.*, *4*, 211–239.

Dunne, T. (1990), Hydrology, mechanics, and geomorphic implications of erosion by subsurface flow, in *Groundwater Geomorphology: The Role of Subsurface Water in Earth-Surface Processes and Landforms*, edited by C. G. Higgins and D. R. Coates, *Spec. Pap. Geol. Soc. Am.*, *252*, 1–28.

Flores-Cervantes, J. H., E. Istanbulluoglu, and R. L. Bras (2006), Development of gullies on the landscape: A model of headcut retreat resulting from plunge pool erosion, *J. Geophys. Res.*, *111*, F01010, doi:10.1029/2004JF000226.

Fowler, A. C., N. Kopteva, and C. Oakley (2007), The formation of river channels, *Siam J. Appl. Math.*, *67*(4), 1016–1040.

Fox, G. A., G. V. Wilson, R. K. Periketi, and B. F. Cullum (2006), A sediment transport model for seepage erosion of streambanks, *J. Hydraul. Eng.*, *11*, 603–611.

Fox, G. A., M. Chu-Agor, and G. V. Wilson (2007), Erosion of noncohesive sediment by ground water seepage: Lysimeter experiments and stability modeling, *Soil Sci. Soc. Am. J.*, *71*, 1822–1830, doi:10.2136/sssaj2007.0090.

Gomez, B., and V. T. Mullen (1992), An experimental study of sapped drainage network development, *Earth Surf. Processes Landforms*, *17*, 465–476.

Higgins, C. G. (1982), Drainage systems developed by sapping on Earth and Mars, *Geology*, *10*, 147–152.

Higgins, C. G. (1984), Piping and sapping: Development of landforms by groundwater outflow, in *Groundwater as a Geologic Agent*, edited by R. G. LaFleur, pp. 18–58, Allen and Unwin, Boston, Mass.

Hoke, G. D., B. L. Isacks, T. E. Jordan, and J. S. Yu (2004), Groundwater-sapping origin for the giant quebradas of northern Chile, *Geology*, *32*, 605–608.

Howard, A. D. (1988), Groundwater sapping experiments and modeling, in *Sapping Features of the Colorado Plateau: A Comparative Planetary Geology Field Guide*, edited by A. D. Howard, R. C. Kochel, and H. Holt, *NASA Spec. Publ.*, *SP-491*, 71–83.

Howard, A. D. (1994), A detachment-limited model of drainage basin evolution, *Water Resour. Res.*, *30*(7), 2261–2285.

Howard, A. D. (1995), Simulation modeling and statistical classification of escarpment planforms, *Geomorphology*, *12*, 187–214.

Howard, A. D., and C. F. McLane III (1988), Erosion of cohesionless sediment by groundwater seepage, *Water Resour. Res.*, *24*(10), 1659–1674.

Huang, C., and J. M. Laflen (1996), Seepage and soil erosion for a clay loam soil, *Soil Sci. Soc. Am. J.*, *60*, 408–416.

Istanbulluoglu, E., R. L. Bras, H. Flores-Cervantes, and G. E. Tucker (2005), Implications of bank failures and fluvial erosion for gully development: Field observations and modeling, *J. Geophys. Res.*, *110*, F01014, doi:10.1029/2004JF000145.

Izumi, N. (2004), The formation of submarine gullies by turbidity currents, *J. Geophys. Res.*, *109*, C03048, doi:10.1029/2003JC001898.

Izumi, N., and K. Fujii (2006), Channelization on plateaus composed of weakly cohesive fine sediment, *J. Geophys. Res.*, *111*, F01012, doi:10.1029/2005JF000345.

Izumi, N., and G. Parker (1995), Inception of channellization and drainage basin formation: Upstream-driven theory, *J. Fluid Mech.*, *283*, 341–363.

Izumi, N., and G. Parker (2000), Linear stability analysis of channel inception: Downstream-driven theory, *J. Fluid Mech.*, *419*, 239–262.

Kirkby, M. J., and L. J. Bull (2000), Some factors controlling gully growth in fine-grained sediments: A model applied in southeast Spain, *Catena*, *40*, 127–146.

Kirkby, M. J., L. J. Bull, J. Poesen, J. Nachtergaele, and L. Vanderkerckhove (2003), Observed and modeled distributions of channel and gully heads with examples from SE Spain and Belgium, *Catena*, *50*, 415–434.

Kochel, R. C., and J. F. Piper (1986), Morphology of large valleys on Hawaii: Evidence for groundwater sapping and comparisons with Martian valleys, *Proc. Lunar Planet Sci. Conf. 17th*, Part 1, *J. Geophys. Res.*, *91*, suppl., E175–E192.

Kooi, H., and C. Beaumont (1996), Large-scale geomorphology: Classical concepts reconciled and integrated with contemporary ideas via a surface processes model, *J. Geophys. Res.*, *101*(B2), 3361–3386.

Laity, J. E., and M. C. Malin (1985), Sapping processes and the development of theatre-headed valley networks on the Colorado Plateau, *Geol. Soc. Am. Bull.*, *96*, 203–217.

Lamb, M. P., A. D. Howard, J. Johnson, K. X. Whipple, W. E. Dietrich, and J. T. Perron (2006), Can springs cut canyons into rock?, *J. Geophys. Res.*, *111*, E07002, doi:10.1029/2005JE002663.

Lamb, M. P., W. E. Dietrich, and J. G. Venditti (2008), Is the critical Shields stress for incipient sediment motion dependent on channel-bed slope?, *J. Geophys. Res.*, *113*, F02008, doi:10.1029/2007JF000831.

Lobkovsky, A. E., B. Jensen, A. Kudrolli, and D. H. Rothman (2004), Threshold phenomena in erosion driven by subsurface flow, *J. Geophys. Res.*, *109*, F04010, doi:10.1029/2004JF000172.

Lobkovsky, A. E., B. E. Smith, A. Kudrolli, D. C. Mohrig, and D. H. Rothman (2007), Erosive dynamics of channels incised by subsurface water flow, *J. Geophys. Res.*, *112*, F03S12, doi:10.1029/2006JF000517.

Loewenherz, D. S. (1991), Stability and the initiation of channelized surface drainage: A reassessment of the short wavelength limit, *J. Geophys. Res.*, *96*(B5), 8453–8464.

Loewenherz-Lawrence, D. S. (1994), Hydrodynamic description for advective sediment transport processes and rill initiation, *Water Resour. Res.*, *30*(11), 3203–3212.

Luke, J. C. (1974), Special solutions for nonlinear erosion problems, *J. Geophys. Res.*, *79*(26), 4035–4040.

Luo, W. (2000), Quantifying groundwater-sapping landforms with a hypsometric technique, *J. Geophys. Res.*, *105*(E1), 1685–1694.

Luo, W., and A. D. Howard (2008), Computer simulation of the role of groundwater seepage in forming Martian valley networks, *J. Geophys. Res.*, *113*, E05002, doi:10.1029/2007JE002981.

Osman, A. M., and C. R. Thorne (1988), Riverbank stability analysis. I: Theory, *J. Hydraul. Eng.*, *114*, 134–150.

Owoputi, L. O., and W. J. Stolte (2001), The role of seepage in erodibility, *Hydrol. Processes*, *15*, 13–22.

Perron, J. T., W. E. Dietrich, and J. W. Kirchner (2008), Controls on the spacing of first-order valleys, *J. Geophys. Res.*, *113*, F04016, doi:10.1029/2007JF000977.

Perron, J. T., J. W. Kirchner, and W. E. Dietrich (2009), Formation of evenly spaced ridges and valleys, *Nature*, *460*, 502–505, doi:10.1038/nature08174.

Pillans, B. (1985), Drainage initiation by subsurface flow in South Taranaki, New Zealand, *Geology*, *13*, 262–265.

Pornprommin, A., N. Izumi, and T. Tsujimoto (2009), Channelization on plateaus with arbitrary shapes, *J. Geophys. Res.*, *114*, F01032, doi:10.1029/2008JF001034.

Revelli, R., and L. Ridolfi (2001), Inception of channelization over a non-flat bed, *Meccanica*, *35*(5), 457–461.

Roering, J. J., J. W. Kirchner, and W. E. Dietrich (1999), Evidence for nonlinear, diffusive sediment transport on hillslopes and implications for landscape morphology, *Water Resour. Res.*, *35*(3), 853–870.

Schorghofer, N., B. Jensen, A. Kudrolli, and D. H. Rothman (2004), Spontaneous channelization in permeable ground: Theory, experiment, and observation, *J. Fluid Mech.*, *503*, 357–374.

Schumm, S. A., and L. Phillips (1986), Composite channels of the Canterbury Plain, New Zealand: A Martian analog?, *Geology*, *14*, 326–329.

Schumm, S. A., M. D. Harvey, and C. C. Watson (1984), *Incised Channels: Morphology, Dynamics and Control*, 200 pp., Water Resour., Littleton, Colo.

Schumm, S. A., K. F. Boyd, C. G. Wolff, and W. J. Spitz (1995), A groundwater sapping landscape in the Florida panhandle, *Geomorphology*, *12*, 281–297.

Smith, T. R., and F. P. Bretherton (1972), Stability and the conservation of mass in drainage basin evolution, *Water Resour. Res.*, *8*(6), 1506–1529.

Sultan, N., et al. (2004), Triggering mechanisms of slope instability processes and sediment failures on continental margins: A geotechnical approach, *Mar. Geol.*, *213*, 291–321.

Tucker, G. E., and R. L. Bras (1998), Hillslope processes, drainage density, and landscape morphology, *Water Resour. Res.*, *34*(10), 2751–2764.

Wilson, G. V., R. Periketi, G. A. Fox, S. Dabney, D. Shields and R. F. Cullum (2007), Seepage erosion properties contributing to streambank failure, *Earth Surf. Processes Landforms*, *32*, 447–459.

N. Izumi, Department of Civil Engineering, Hokkaido University, Nishi 8, Kita 13, Kita-ku, Sapporo, Hokkaido 060-8628, Japan. (nizumi@eng.hokudai.ac.jp)

A. Pornprommin, Department of Water Resources Engineering, Kasetsart University, 50 Phahonyothin Rd., Jatujak, Bangkok 10900, Thailand. (fengacp@ku.ac.th)